Measurement of ionospheric TEC in spaceborne SAR Data

Jehle, M ; Frey, O ; Small, David ; Meier, E

DOI: https://doi.org/10.1109/TGRS.2010.2040621

Influence of Atmospheric Path Delay on the Absolute Geolocation Accuracy of TerraSAR-X High-Resolution Products

Adrian Schubert, Michael Jehle, *Student Member, IEEE*, David Small, *Member, IEEE*, and Erich Meier, *Member, IEEE*

***Abstract*—Two coupled investigations of TerraSAR-X (TSX) high-resolution data are described in this paper: geometric validation, and estimation of the tropospheric path delay using measurements of corner reflectors (CRs) placed at different altitudes but nearly identical ranges. The CRs were placed within Alpine and valley sites in Switzerland, where terrain diversity provides ideal territory for geometric validation studies. Geometric validation was conducted using slant-range complex products from the spotlight and stripmap (SM) modes in ascending and descending configurations. Based on the delivered product annotations, the CR image positions were *predicted*, and these predictions were compared to their *measured* image positions. To isolate path delays caused by the atmosphere, six TSX SM scenes ($\sim 35 \times 50$ km) were examined containing four identical CRs with the same ranges and an altitude difference of $\sim$3000 m. The CR arrangement made it possible to verify the annotated TSX atmospheric path delay by comparing the predicted slant range with the slant range obtained by measuring the reflector image coordinates. Range differences between the high- and low-altitude reflectors helped to quantify small variations in the path delay. Both SM and spotlight TSX products were verified to meet the specified accuracy requirements, even for scenes with extreme terrain variations, in spite of the simplicity of the atmospheric model currently integrated into the processor. Small potential improvements of the geolocation accuracy through the implementation of more comprehensive atmospheric modeling were demonstrated.**

***Index Terms*—Atmospheric path delay, synthetic aperture radar geometry, TerraSAR-X (TSX).**

I. Introduction

TERRASAR-X (TSX) is the first civilian spaceborne radar satellite with the ability to observe the Earth with a resolution on the order of $\sim$1 m. With the aim of quantifying its geolocation accuracy, TSX scenes were acquired over Switzerland between February and August 2008 using the high-resolution spotlight (HS) and stripmap (SM) modes, and single-look slant-range complex (SSC) products were ordered. All had "science" quality (SCIE) orbits, with the exception of two HS products delivered with "rapid" orbit (RAPD) accuracy (descending geometry, Zurich test site). The products were initially terrain geocoded using the best available digital height model (DHM) for each scene [9]; this was either a Swiss 25-m digital terrain model (DTM) or a digital surface model (DSM) obtained from LIDAR. By draping the geocoded images over reference layers such as a 1 : 25 000 topographic map or the DHM used during geocoding, the global consistency and coarse registration accuracy of the products was confirmed. Fig. 1 shows two examples of such overlays: (a) an SM product over the Alps ($\sim 35 \times 50$ km) and (b) an HS product over the city of Meiringen ($\sim 10 \times 5$ km), also visible in the northwestern part of the SM image. Further examples are given in [9].

For the validation of TSX's absolute geolocation accuracy, given its resolution of $\sim$1 m, the effect of the atmosphere—particularly the troposphere—needs to be considered. The tropospheric path delay is caused by *hydrostatic* (air pressure), *wet* (water vapor), and *liquid* (water droplet) variations. The TSX SSC product annotations contain a single total path delay and a constant azimuth timing offset estimate. Note that the product slant range and azimuth timing annotations are not themselves adjusted [2] but are applied together with an atmospheric model in our geolocation processor. The inherent *product* geolocation accuracy is given by the adjusted timing values. By situating trihedral corner reflectors (CRs) at different altitudes and imaging these sites using TSX's SM and HS modes, the attained geometric accuracy of the delivered products was measured. Suitably placed high- and low-altitude reflectors provided further indications of the magnitude of the path delay at different heights.

II. Acquisition Geometry

Nine trihedral CRs with side lengths of 80 cm were placed within five Swiss midland sites and one Alpine site (Zurich, Malters, Rohrdorf, Meiringen, Interlaken, and Jungfraujoch, respectively), shown in Fig. 2. The CR positions were estimated to approximately centimeter accuracy with differential GPS (DGPS) surveys. In each case, a CHTRF95 reference station was always nearby, reducing the theoretical pure-DGPS positioning accuracy to $\sim$1–2 cm (as reflected by the standard deviation of the GPS measurements collected typically over a period of $\sim$40 min). The additional manual measurement of the vertical offset between CR and GPS antenna phase centers was estimated to introduce no more than $\sim$1–2 cm maximum, resulting in total expected errors well under $\sim$10 cm. The CRs at

Manuscript received February 28, 2009; revised June 18, 2009 and September 12, 2009. First published December 22, 2009; current version published January 20, 2010. This work was supported in part by the German Aerospace Center (DLR) within the framework of the calibration/validation project CAL0163.

The authors are with the Remote Sensing Laboratories, University of Zurich, 8057 Zurich, Switzerland (e-mail: adrian.schubert@geo.uzh.ch; michael.jehle@geo.uzh.ch; david.small@geo.uzh.ch; erich.meier@geo.uzh.ch).

Digital Object Identifier 10.1109/TGRS.2009.2036252

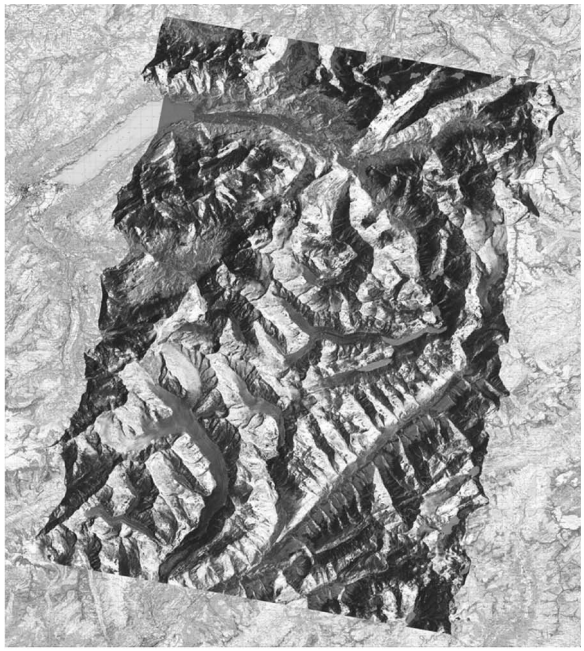

(a) Stripmap product from 2008/04/28

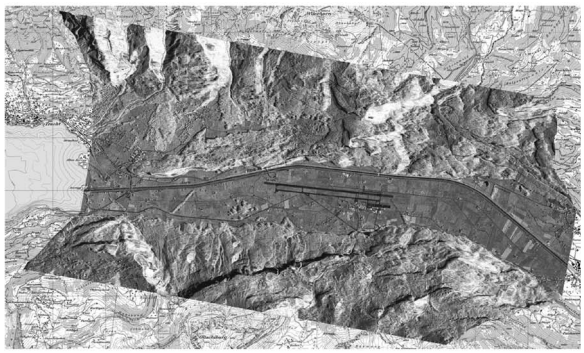

(b) High-resolution Spotlight product from 2008/08/27

Fig. 1. Terrain-geocoded SM and HS products over (a) Alps surrounding Meiringen/Jungfraujoch and (b) Meiringen airport. Maps Swisstopo.

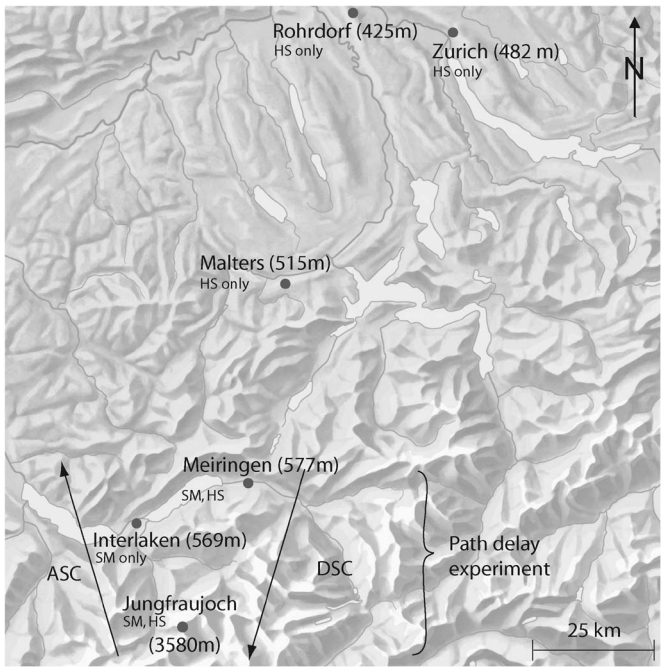

Fig. 2. Test sites and product types acquired (SM and HS). Acquisition geometry for the path delay experiment in the Bernese Oberland (Meiringen/Interlaken/Jungfraujoch) is indicated near the lower left part of the image.

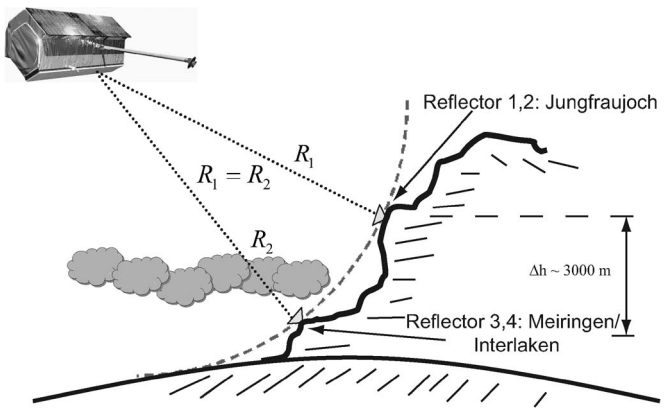

Fig. 3. Observation geometry for the path delay experiment.

all six test sites were used as geolocation test points; the three southernmost sites (Meiringen, Interlaken, and Jungfraujoch) in the Bernese Highlands were specifically selected for the path delay experiment (indicated in Fig. 2).

Fifteen acquisitions were made in total: seven in the SM mode and eight in the HS mode. The path delay experiment included HS and SM products; the sites Zurich, Malters, and Rohrdorf were added as additional HS-only sites. The inclusion of high-altitude reflectors at Jungfraujoch served two purposes: validating TSX's geometric accuracy for a range of terrain altitudes after the incorporation of the nominal atmospheric annotations and quantifying the influence of the atmosphere on the signal path.

To isolate the path delay effect for the selected CR measurements, pairs of trihedral CRs were placed in the three Bernese Highlands sites, with the reflectors from each pair equidistant to the sensor (to within ∼10 m) but at significantly different altitudes. As illustrated in Fig. 3, reflectors were placed at ∼3580 m altitude (Jungfraujoch), and in the valley below at ∼570 m (Meiringen for descending orbits, Interlaken for ascending orbits). The high-altitude reflector measurements were subjected to less atmospheric interference than their valley homologues ∼3 km lower. Although each pair of CRs was separated by ∼20 km along the flight track, the effect of the different atmospheric depths along the signal path is assumed here to be much greater than possible along-track atmospheric variations over this short distance (up to ∼10-cm path delay variation). Two pair configurations were installed to accommodate the ascending and descending orbits, with four reflectors visible in each scene (two high-altitude ones and two low-altitude ones) for redundancy.

With this arrangement, the nominal TSX correction scheme for the atmospheric path delay was tested by comparing the predicted and measured ranges, as described in the following.

III. CR Measurements

Given the radar timing annotations (time of first range sample, range sampling rate, first azimuth time, and azimuth sample interval) and the state vectors describing the satellite's

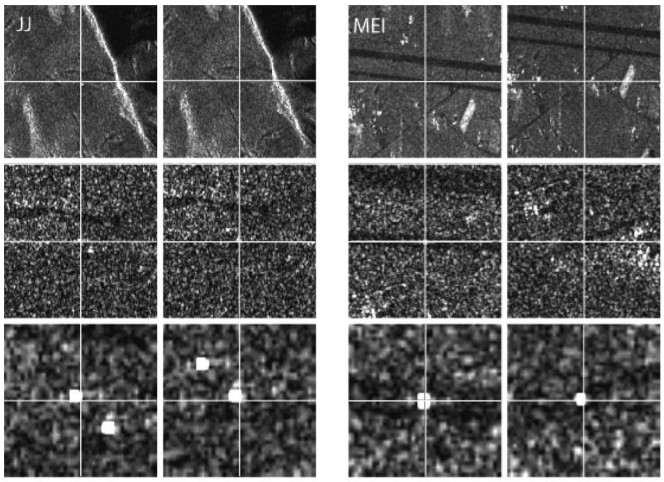

Fig. 4. CRs as seen in two geocoded images at three zoom levels for the sites (a) Jungfraujoch and (b) Meiringen. The crosshairs represent the predictions based on the CR GPS measurements.

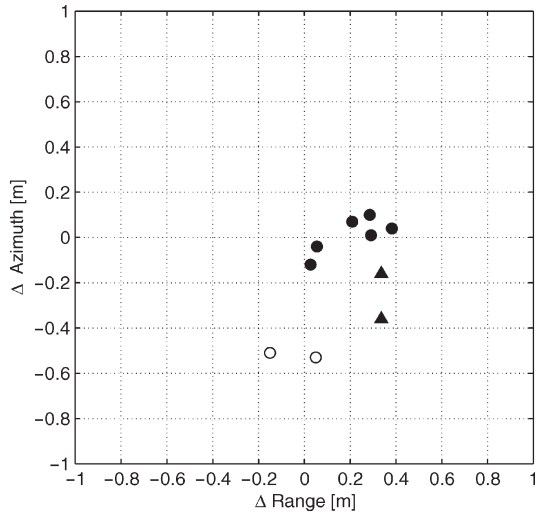

Fig. 5. Spotlight (HS) products: Absolute location error scatter plot for ten CRs in eight Alpine and low-altitude scenes. Solid markers indicate descending geometry; hollow markers indicate ascending geometry. Triangles represent the high-altitude CRs at Jungfraujoch; all other symbols represent the CRs at low-altitude sites.

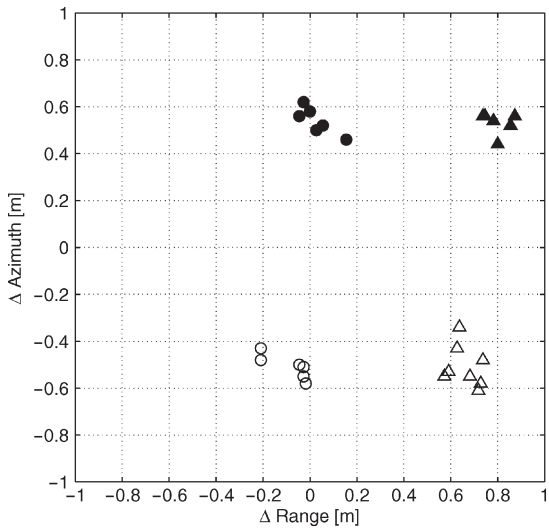

Fig. 6. SM products: Absolute location error scatter plot for 26 CRs at the Alpine and valley test sites in seven products. Solid markers indicate descending geometry; hollow markers indicate ascending geometry. Triangles represent the high-altitude CRs at Jungfraujoch; all other symbols represent the CRs at valley sites.

trajectory during the time of data acquisition, a point on the Earth's surface may be located within the image by solving the Doppler equation governing the image product's geometry. This involves searching for the azimuth time where the satellite's position corresponds to the required Doppler value (typically zero). This geolocation method is called "range Doppler" [5].

The surveyed locations of the CRs were predicted within the radar image products. Additional corrections were made for the atmospheric path delay and a constant azimuth timing shift, with both indicated in the annotations for the geolocation grid (GEOREF.xml). The predicted coordinates were then compared to their measured positions. This is illustrated in Fig. 4 for reflectors within three of the test sites. In each case, the target's predicted image location is marked with a cross, the result of transforming the GPS coordinate of the CR phase center into the slant-range image coordinates. The zoom level increases toward the bottom.

The HS images, with their submeter sample spacing, provide the best opportunity to precisely locate reflector peak returns. Using complex fast Fourier transform oversampling, the location of a given reflector is determined as the local intensity maximum with subpixel accuracy [10]. The slant range from the sensor to the reflector is then obtained using the range timing annotations, taking into account the additional range offset due to the atmospheric path delay, indicated in the product annotations. Since the atmospheric model calculates a single delay for the scene based on a mean reference height, it is *expected* that path delay variations due to different CR altitudes should cause residual range location errors. Indeed, this effect is visible for the high- versus low-altitude CRs in Figs. 5 and 6, which show the *predicted* minus the *measured* CR positions, henceforth called the "location error."

Fig. 5 summarizes the location error estimates for all reflectors in eight HS products received. The solid markers indicate the descending products; the hollow markers indicate the ascending products. The triangles represent the Jungfraujoch (high-altitude Alpine) reflectors and the circular markers the low-altitude (valley or lowland) reflectors. Azimuth and range errors alike were all within ∼0.5 m. A small positive bias of 0.18 m is apparent in the range errors, although the number of measurements is too small to assign much significance to this shift. A separation is additionally visible between ascending and descending scenes (indicated by the hollow and solid markers, respectively), although here, more ascending measurements would help clarify this tendency.

The current specifications for the TSX products generated from SCIE and RAPD orbits are listed in [2, Sec. 3.4]; it is also claimed that both orbit types are accurate to within 20 cm (even RAPD, in spite of its stated 2-m tolerance). The absolute geometric accuracy—including all uncertainties in the signal path and along-track errors—is stated to be within 1 m (with one-sigma uncertainty). The measurements made using the CRs

in the HS scenes support this claim in both the slant range and azimuth directions.

The equivalent geolocation errors for all six SM scenes containing high-/low-altitude reflector pairs (plus one extra SM scene with only two Alpine CRs available) are shown as a scatter plot in Fig. 6. Even with the altitude differences of up to ∼3 km and the use of the single annotated atmospheric path delay, all errors are well under 1 m, within the product accuracy specifications. The main residual effects that we observe are the following: 1) an azimuth separation of ∼1 m between ascending and descending acquisitions, symmetric about zero; 2) a range separation of ∼0.8 m between Alpine and valley measurements; and 3) a positive mean range error bias of ∼0.4 m for the measurements on the whole.

Effect 2) can be explained by considering the location of the scene reference height relative to the CR altitudes. The average scene height in both configurations was approximately equidistant between the mountain and valley positions. This should imply that, if the operational path delay estimate is calculated for the reference height, the high-altitude slant ranges would be overcorrected slightly and the low-altitude ranges undercorrected. That is, the measured range location errors would be expected to be of similar magnitude and opposite sign for the valley sites in comparison to the high-altitude site. While not symmetric about zero (effect 3) listed earlier), the ∼0.8-m separation between high- and low-altitude measurements corresponds well to an altitude-dependent path delay over- and undercorrection.

Comparing Fig. 6 to Fig. 5, the increased spread in the range error values in the former can partly be explained by the differences in the reflector altitudes and the annotated product's mean scene heights. Due to their smaller areal extent, for the HS products studied, the annotated scene average terrain heights more closely represent the CR altitudes than is the case for the SM products. This likely reduced the range errors stemming from the altitude differences, decreasing their spread in the HS case in comparison to SM.

IV. Atmospheric Path Delay From Annotations

The TSX operational processor provides a single path delay estimate and a constant azimuth timing shift for the whole scene in question. The path delay value is based on the influence of the ionosphere and the troposphere using the average total electron content values, the average scene height, and the midrange incidence angle [3], [4]. These offsets were initially subtracted from the range (fast) and azimuth (slow) times, respectively, to ideally simulate vacuum conditions, resulting in Figs. 5 and 6. However, the provided path delay constant is estimated at the average scene height; atmosphere-induced geolocation errors of up to ∼1 m can be expected in steep mountainous terrain. For example, if only a small fraction of the scene contains mountainous terrain, the resulting low mean scene height will cause local overcompensation of the path delay of up to ∼1 m in the mountains, depending on the atmospheric conditions.

Estimates of the altitude-dependent path delay were calculated from the offsets between predicted and measured CR peak locations. The results of this analysis are presented in Table I. To do this for a given site, the measured range displacement ($\Delta\mathrm{Rg}$; Note: average of two reflectors at each site) was subtracted from the annotated delay given for the scene average height Ψ_{AVG}. The estimated delays for the Alpine and valley sites are listed in the columns $\varphi_{\mathrm{JJ,AVG}}$ and $\varphi_{\mathrm{MI,AVG}}$, respectively. The high-altitude range delays $(\varphi_{\mathrm{JJ,AVG}})$ are lower than the valley delays $(\varphi_{\mathrm{MI,AVG}})$, as expected, due to the greater path delay in the valley cases (mainly occurring in the troposphere). The rightmost column $(\varphi_{\mathrm{MI}} - \varphi_{\mathrm{JJ}})$ lists the difference between the two previous columns, i.e., the path delay difference between the high- and low-altitude locations.

TABLE I
Predicted Path Delay From Measurements and GPS

Date (2008)	A/D	Ref. Height [m]	θ_i [°]	Ψ_{AVG} [m]	ΔRg_{JJ} [m]	ΔRg_{MI} [m]	$\varphi_{JJ,AVG}$ [m]	$\varphi_{MI,AVG}$ [m]	φ_{MI}- φ_{JJ} [m]
28.04	D	2163	32.06	1.874	0.791	0.091	1.08	1.78	0.70
09.05	D	2166	32.56	1.873	0.742	-0.036	1.13	1.91	0.78
12.05	A	1865	24.68	1.845	0.710	-0.036	1.14	1.88	0.74
23.05	A	1827	24.67	1.857	0.723	-0.023	1.13	1.88	0.75
11.06	D	2164	32.06	1.874	0.864	0.028	1.01	1.85	0.84
25.06	A	1827	24.66	1.857	0.632	-0.209	1.23	2.07	0.84
Mean Values				1.863	0.744	-0.031	1.12	1.90	0.78

Ref. Height and Ψ_{AVG} refer to the mean scene height and scene-average path delay, respectively, as annotated in the TSX products; θ_i is the mean local incidence angle (JJ: Jungfraujoch, MI: Meiringen / Interlaken). Path delay predictions (φ) for the JJ and MI sites are given by the differences between measured and predicted CR ranges (ΔRg). All scenes acquired in 2008.

A previous work [4] reported on the altitude dependence of the path delay using ray-tracing simulations within a numerical weather model, as well as a simpler height-dependent atmospheric model. It was discovered that the measured range deviations closely followed the dynamics of the predictions from both atmospheric models. After investigating the applicability of the TSX model to midlatitudes, it was concluded that the scene average path delay (Ψ_{AVG}) from the TSX annotations was consistently underestimated by ∼0.35 m in the products tested at these latitudes. If the underestimation were corrected (i.e., Ψ_{AVG} were increased by ∼0.35 m), then the measured range location errors $(\Delta\mathrm{Rg})$ would similarly be expected to improve (decrease) by 0.35 m, shifting the contents in Fig. 6 to the left and causing them to become approximately symmetric about zero, as initially had been expected.

V. Path Delay Correction Using Improved Atmospheric Modeling

If one wishes to remove the atmospheric effects from the CR measurements to isolate the remaining effects, a more accurate atmospheric model needs to be used. The tropospheric model implemented in the operational TSX processor is described in [3]. Using this model, an improvement to the error measurements in Figs. 5 and 6 was made by recalculating the path delay for the height of each CR. The new path delays were then substituted for the scene average delay annotated in the TSX products, and the range errors in Figs. 5 and 6 were recalculated. Beginning with the range errors measured using the TSX path delay corrections, the *differences* between the scene average path delays and the height-dependent delays were

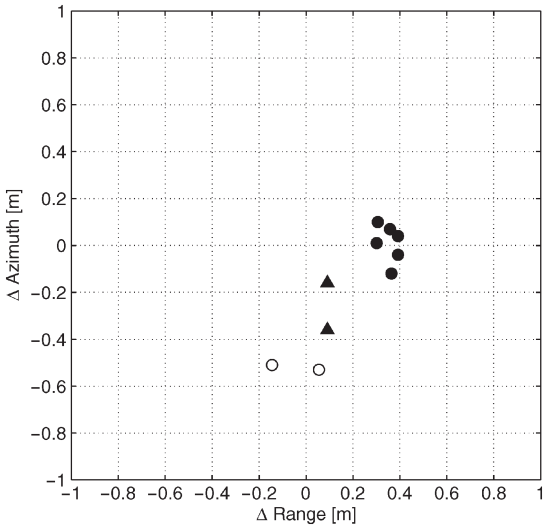

Fig. 7. Spotlight (HS) products: Absolute location error scatter plot using the TSX atmospheric model with true CR heights. Solid markers indicate descending geometry and hollow markers ascending geometry. Triangles represent the CRs at Jungfraujoch and circles the CRs at low-altitude sites.

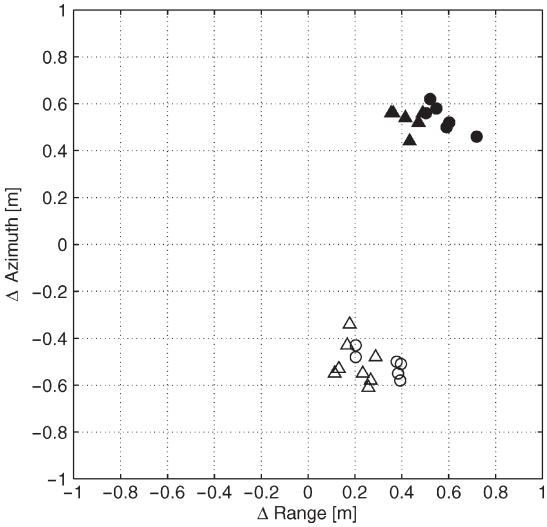

Fig. 8. SM products: Absolute location error scatter plot using the TSX atmospheric model with true CR heights. Solid markers indicate descending geometry and hollow markers ascending geometry. Triangles represent the CRs at Jungfraujoch and circles the CRs at valley sites.

subtracted from the old range errors, yielding the errors that would have resulted using the TSX model in conjunction with local CR heights

$$\Delta \mathrm{R}_{\mathrm{CR}} = \Delta \mathrm{R}_{\mathrm{AVG}} - (\Psi_{\mathrm{AVG}} - \Psi_{\mathrm{CR}}) \tag{1}$$

where

$\Delta \mathrm{R}_{\mathrm{CR}}$ range error estimate using the delay from the TSX processor model given the local CR height;

$\Delta \mathrm{R}_{\mathrm{AVG}}$ range error estimate using the TSX-annotated scene average path delay;

Ψ_{AVG} TSX-annotated scene average path delay;

Ψ_{CR} path delay using the TSX processor model for a given CR.

The resulting adjusted location errors are shown in Figs. 7 and 8 for the HS and SM cases, respectively. The most notable change is the clear decrease in the range differences between low- and high-altitude reflectors, particularly in the SM case (Fig. 8). These results simulate the geolocation accuracy that is achievable using the current TSX atmospheric model along with a DTM.

Next, we wished to further isolate the range geolocation accuracy from atmospheric interference by using a more physically accurate atmospheric model. In [4], a model that depends on ray tracing through a variable refractivity field is described and defined. It was determined to provide the most accurate path delay estimates and thus served as a reference in this study. Using this model, the total atmospheric (including the ionosphere) path delay was calculated for each imaged CR. Adjustments to the $\Delta \mathrm{R}_{\mathrm{CR}}$ results were made as described previously for the height-dependent TSX model (1).

For the HS measurements only, the ray tracer values were not available due to campaign-related organizational restrictions; an atmospheric model incorporating data from local weather stations was used instead. It also takes local incidence angle, pressure, and temperature effects into account and was determined to be consistent with the ray tracer estimates (for the SM reflectors) to within $\sim$8 cm.

Using the best available atmospheric model to correct for the expected path delays, the adjusted error plots are provided in Figs. 9 and 10 for the HS and SM scenes, respectively. Comparing the adjusted SM measurements (Fig. 10) to the original measurements (Fig. 6), the gap in the range errors between the valley and Alpine CRs has been virtually eliminated, with an approximate threefold reduction in the standard deviation in the range dimension. As expected, modeling the atmosphere for specific scene points (i.e., modeling the specific path from the CR to the sensor) greatly reduces the offsets in range between the predicted and measured CR positions. The HS range errors in Fig. 9 also changed in comparison to their previous values in Fig. 5, but no significant improvement in the point cloud density is visible. As previously discussed, this is probably because of the closer correspondence between the scene average height and the true CR altitudes for the smaller HS scenes.

VI. Discussion

Referring to the atmosphere-corrected HS and SM cases in Figs. 9 and 10, clear range error offsets remain. The mean range error offset in the HS case is 0.48 m; for SM, the mean is 0.71 m. These offsets are likely caused by an error in the range gate [or sampling window start time (SWST)] bias. As noted in [6, Appendix II.C], the SWST bias estimation is coupled to the atmospheric model during initial calibration/validation of the instrument, as both contribute to the measured signal delay. If an erroneous atmospheric model is used during initial instrument calibration, the SWST bias estimate is inherently calibrated to compensate for the initially incorrect atmospheric bias. Consequently, if the atmospheric model is later corrected—as simulated in this investigation—one *expects* to see a residual range bias reflecting the miscalibration in the old SWST bias.

In the current investigation, the annotated path delay is derived from a simple atmospheric model that may additionally

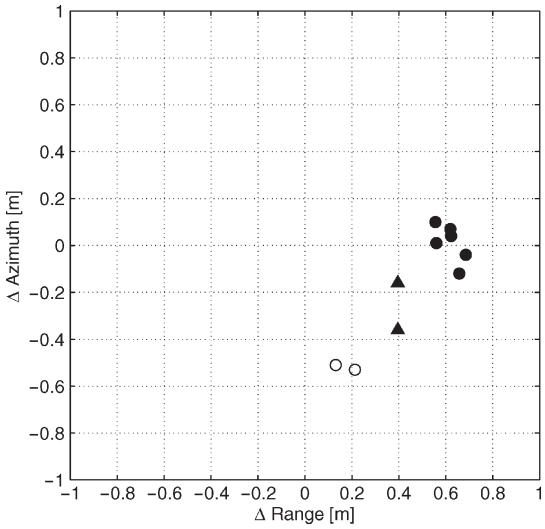

Fig. 9. Spotlight (HS) products: Absolute location error scatter plot for the CRs using an improved atmospheric model. Solid markers indicate descending geometry and hollow markers ascending geometry. Triangles represent the CRs at Jungfraujoch and circles the CRs at low-altitude sites.

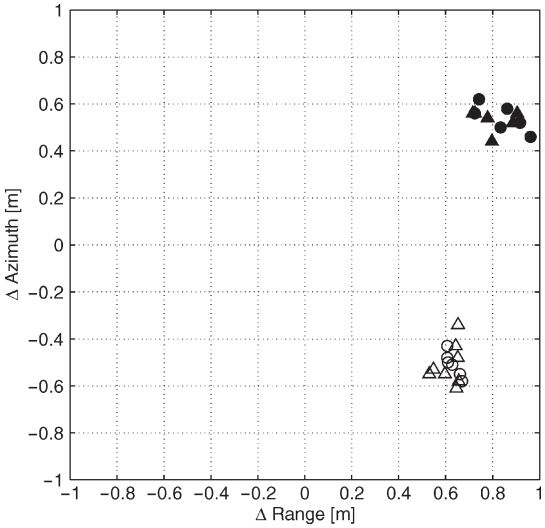

Fig. 10. SM products: Absolute location error scatter plot for the CRs using an improved atmospheric model. Solid markers indicate descending geometry and hollow markers ascending geometry. Triangles represent the CRs at Jungfraujoch and circles the CRs at valley sites.

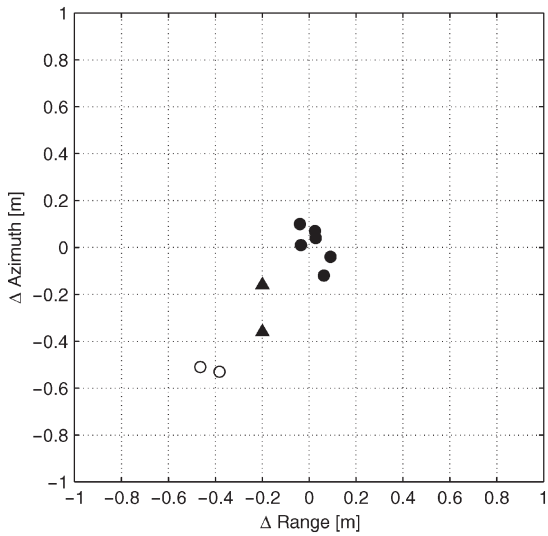

Fig. 11. Absolute location error scatter plot for the CRs in the HS scenes with a hypothetical SWST bias shift of 0.60 m subtracted from the data. Solid markers indicate descending geometry and hollow markers ascending geometry. Triangles represent the CRs at Jungfraujoch and circles the CRs at low-altitude sites.

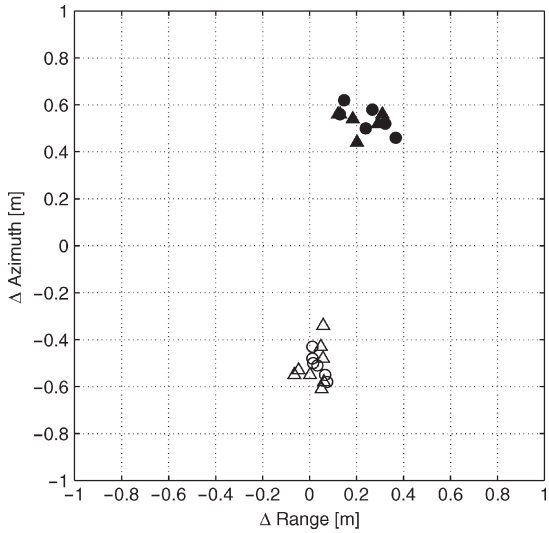

Fig. 12. Absolute location error scatter plot for the CRs in the SM scenes with a hypothetical SWST bias shift of 0.60 m subtracted from the data. Solid markers indicate descending geometry and hollow markers ascending geometry. Triangles represent the CRs at Jungfraujoch and circles the CRs at low-altitude sites.

not be optimized for mid-latitudes; thus, it is plausible that the initial SWST bias calibration (coupled to the path delay values) was subject to an error that is equal approximately to the magnitude of the measured offsets in Figs. 9 and 10, i.e., a value between $\sim$0.5 and $\sim$0.7 m.

If such an SWST bias error exists, it can be adjusted in the TSX processor (the improvement in tiepoint-free geolocation accuracy following the European Space Agency's SWST bias calibration for Envisat ASAR is shown in [11]). If a revised SWST bias is calculated as the mean of the SM and spotlight biases, a value of 0.60 m is obtained. If this revised SWST bias offset is used to recalculate the error plots, the range errors appear as shown in Figs. 11 and 12 for HS and SM, respectively. The remaining mean offsets are reduced in comparison to those in Figs. 9 and 10: -0.12 m for the spotlight case (Fig. 11) and 0.11 m in the SM case (Fig. 12).

The last remaining prominent effect—most distinctly visible in the SM products—is the symmetric azimuth error separation between ascending and descending CR measurements. At first glance, this would seem to be due to a consistent southward bias of $\sim$0.5 m in the CR positions, which would place the imaged CR *further* along track than predicted in the descending case and *earlier* along track in the ascending case. Given the descending geometry, the azimuth prediction would be 0.5 m *after* the true location, resulting in a positive error. This hypothesis is highly unlikely, as multiple DGPS measurements were made

using proven techniques and instrumentation, and utilizing an assortment of differential reference stations, dependent on each test site location.

Positional errors could also result from a difference in the reference frames (i.e., data) defined for the DGPS measurements versus the TSX orbital state vectors; this would be equivalent to a constant error in the CR positions. The reference frame used for the orbit state vectors is WGS84-G1150 (defined in [7]) according to the TSX product annotations (format described in [1]). WGS84-G1150 and the international reference frame ITRF are identical to within approximately several centimeters at most, according to [7] and [8] (although no documentation of the relationship is publicly available). GPS measurements of the CRs were made within the CHTRF95 reference frame, which is coupled to the Eurasian continental plate, described by ETRF89 epoch 1993. ETRF89 is, in turn, coupled to ITRF epoch 1989 (see [8] for details). ETRF drifts at a rate of ~2–3 cm/year toward the northeast with respect to the ITRF; the total relative drift since 1989 is nearly 50 cm. Initial estimates confirm that the reference frame drift appears to partly explain the azimuth separation between the error measurements from ascending and descending acquisitions, as well as partly explain their differing range biases. However, since the relationship between ITRF and WGS84 is not publicly documented with centimeter accuracy and the effect of the relative drift between CHTRF95 and the state vector reference frame is still being investigated, the improvements to the measurements cannot yet be accurately quantified.

Additionally, a constant azimuth shift parameter is provided in the TSX product annotations [1], stated to take "relativistic Doppler" and "internal timing effects" into account. It may also require further adjustment; further collaboration and subsequent calculations will be required to resolve the issue.

While these may prove to be fruitful investigations, it is nonetheless not clear why the HS azimuth errors are not symmetric about zero (although the only two ascending measurements are at the lower end of the data set, consistent with the SM data, at ~ -0.5 m). The cause(s) of the azimuth error distributions remain under investigation.

VII. Summary of Geometric Performance

The geolocation errors for the various atmospheric correction schemes are summarized in Table II. Four columns are shown in the right half, representing the following: 1) the current TSX processor; 2) the current TSX processor, with local CR altitudes substituted for the average scene height, simulating the use of a digital elevation model (DEM); 3) the best available atmospheric model (ray tracing for the SM mode and a weather-dependent physical model for the HS mode); and 4) the best available model, with adjustment for a single hypothetical SWST bias correction. The values are listed according to the acquisition mode (SM/HS) and the orbit direction (ASC/DSC).

It should be noted that column (2) represents the quality achievable with the current operational TSX atmospheric model and the addition of a DTM (i.e., the use of true terrain heights instead of a mean height for the scene).

TABLE II
TSX-1 Geolocation Error Summary

Mode	Orbit type	N	Axis	Current TSX model (Fig. 5-6)	TSX model + DEM (Figs. 7-8)	Best model (Figs. 9-10)	Best model + SWST shift (Fig. 11-12)
HS	ASC	2	rg	-0.05 ± 0.14	-0.05 ± 0.14	0.17 ± 0.06	-0.42 ± 0.06
			az	-0.52 ± 0.01	-0.52± 0.01	-0.52 ± 0.01	-0.52 ± 0.01
	DSC	8	rg	0.24 ± 0.13	0.29 ± 0.13	0.56 ± 0.11	-0.03 ± 0.11
			az	-0.06 ± 0.15	-0.06 ± 0.15	-0.06 ± 0.15	-0.06 ± 0.15
SM	ASC	14	rg	0.34 ± 0.39	0.26 ± 0.10	0.62 ± 0.04	0.03 ± 0.04
			az	-0.51 ± 0.07	-0.51 ± 0.07	-0.51 ± 0.07	-0.51 ± 0.07
	DSC	1 2	rg	0.41 ± 0.41	0.50 ± 0.11	0.82 ± 0.09	0.23 ± 0.09
			az	0.54 ± 0.05	0.54 ± 0.05	0.54 ± 0.05	0.54 ± 0.05

Results are given as mean ± standard deviation [m], based on the corner reflector measurements shown in Figures 5 through 12. N = # measurements.

VIII. Conclusion

The absolute geolocation accuracy of TSX HS and SM products was tested using CRs with surveyed positions. The measurements revealed range errors all well below 1 m. However, a small bias in the range error estimates persisted, probably caused by the application of a model not calibrated for mid-latitudes, that additionally only corrects for one scene-wide reference height.

The measured azimuth errors were also all below 1 m. A clear separation between measurements from ascending and descending acquisitions was observed, particularly for the SM products; the cause is under investigation.

Instead of the TSX product default single path delay estimate per scene, it was shown that the use of the local terrain heights would improve the range geolocation accuracy, particularly for acquisitions over variable terrain.

Estimates based on ray tracing through an atmospheric model consisting of refracting layers lowered the standard deviation of the resulting range geolocation errors by about three times in the SM case, with little change for spotlight measurements. A range error offset of between 50 and 70 cm remains after the improved atmospheric correction, possibly due to an SWST bias initially calibrated in tandem with a suboptimal atmospheric path delay model.

Currently, TSX generates the highest resolution civilian synthetic aperture radar products available, easily meeting its initial accuracy specifications. It is expected that if adjustments were made to the standard atmospheric model currently used (particularly the addition of a DEM), the geometric accuracy of the high-resolution products would further improve.

Acknowledgment

The authors would like to thank B. Scheuchl of Infoterra GmbH for his help in acquiring the HS scenes over the University of Zurich (Irchel campus) and for the permission to use the data in this study; T. Fritz and A. Roth of the German Aerospace Center (DLR), Oberpfaffenhofen, for their scientific support and for providing us with the TSX data sets within the framework of the project CAL0163; International Foundation High Altitude Research Stations Jungfraujoch and Gornergrat (HFSJG), Berne, Switzerland, for making it possible for us to carry out the experiments at Jungfraujoch; the respective airport

authorities for the permission to deploy CRs at the Meiringen and Interlaken airports; Academic Sports Association Zurich (ASVZ) of the University of Zurich for the permission to deploy CRs on their tennis courts; D. Leuenberger of MeteoSwiss for providing the NWP model data; Swisstopo for the Swiss DHM25 and LIDAR DSM over Zurich, both used for terrain geocoding, and for providing 1 : 25 000 reference digital topographic maps; and the reviewers for their valuable suggestions.

REFERENCES

[1] T. Fritz *TerraSAR-X Ground Segment Level 1b Product Format Specification*, Dec. 10, 2007. TX-GS-DD-3307 Iss. 1.3.
[2] T. Fritz and M. Eineder, *TerraSAR-X Ground Segment Basic Product Specification Document*, Feb. 24, 2008. TX-GS-DD-3302 Iss. 1.5.
[3] T. Fritz, H. Breit, and M. Eineder, "TerrSAR-X products—Tips and tricks," in *Proc. 3rd TerraSAR-X Sci. Team Meeting*, Oberpfaffenhofen, Germany, Nov. 25–26, 2008.
[4] M. Jehle, D. Perler, D. Small, A. Schubert, and E. Meier, "Estimation of atmospheric path delays in TerraSAR-X data using models vs. measurements," *Sensors*, vol. 8, no. 12, pp. 8479–8491, 2008.
[5] E. Meier, U. Frei, and D. Nüesch, "Precise terrain corrected geocoded images," in *SAR Geocoding: Data and Systems*, G. Schreier, Ed. Karlsruhe, Germany: Herbert Wichmann Verlag GmbH, 1993, ch. 7.
[6] J. J. Mohr and S. N. Madsen, "Geometric calibration of ERS satellite SAR images," *IEEE Trans. Geosci. Remote Sens.*, vol. 39, no. 4, pp. 842–850, Apr. 2001.
[7] National Imagery and Mapping Agency, *Department of Defense World Geodetic System 1984, and 'Addendum to NIMA TR 8350.2: Implementation of the World Geodetic System 1984 (WGS 84) Reference Frame G1150'*, Jun. 23, 2004. NIMA TR8350.2, Amendment 2.
[8] D. Schneider, E. Gubler, U. Marti, and W. Gurtner, *Aufbau der neuen Landesvermessung der Schweiz 'LV95' Teil 3: Terrestrische Bezugssysteme und Bezugsrahmen*. Wabern, Switzerland: Federal Office Topography, Feb. 2001.
[9] A. Schubert, M. Jehle, D. Small, and E. Meier, "Geometric validation of TerraSAR-X high-resolution products," in *Proc. 3rd TerraSAR-X Sci. Team Meeting*, Oberpfaffenhofen, Germany, Nov. 25–26, 2008.
[10] D. Small, B. Rosich, A. Schubert, E. Meier, and D. Nüesch, "Geometric validation of low- and high-resolution ASAR imagery," in *Proc. ENVISAT, ERS Symp.*, Salzburg, Austria, Sep. 6–10, 2004.
[11] D. Small, B. Rosich, E. Meier, and D. Nüesch, "Geometric calibration and validation of ASAR imagery," in *Proc. CEOS SAR Workshop*, Ulm, Germany, May 27–28, 2004.

Adrian Schubert received the B.Sc. degree in applied physics from the University of Waterloo, Waterloo, ON, Canada, in 1994, the D.E.A. degree in remote sensing from Université Paris 7—Denis Diderot, Paris, France, in 1996, the D.E.S.S. (industry-oriented) degree in geosciences and computing from the University of Paris 6, Paris, in 1997, and the Ph.D. degree in radargrammetry-aided interferometry from the University of Zurich, Zurich, Switzerland, in 2004.

Since 2004, he has been with the Remote Sensing Laboratories, Department of Geography, University of Zurich, working on projects related to SAR geometry and radiometry, sensor calibration and validation, and glacier offset tracking and image matching.

Michael Jehle (S'07) received the Dipl.-Ing. degree in electrical engineering from the University of Karlsruhe, Karlsruhe, Germany, in 2002. He is currently working toward the Ph.D. degree at the University of Zurich, Zurich, Switzerland.

He did scientific project work with the Institute for Very High Frequency Technology and Electronics, University of Karlsruhe, and with the Klinikum für Sportorthopädie, Abteilung Biomechanik, Albert-Ludwigs-Universität Freiburg, Freiburg, Germany. He is currently a Research Assistant with the Remote Sensing Laboratories, University of Zurich. His interests include electromagnetic wave propagation in the atmosphere, signal processing, and SAR systems.

David Small (S'85–M'98) received the B.A.Sc. degree in systems design engineering from the University of Waterloo, Waterloo, ON, Canada, in 1988, the M.A.Sc. degree in electrical engineering from The University of British Columbia, Vancouver, BC, Canada, in 1991, and the Ph.D. degree from the University of Zurich, Zurich, Switzerland, in 1998. In his Ph.D. thesis, he developed a processing chain for generating digital elevation models from repeat-pass ERS data.

He works on SAR geometric and radiometric calibration issues as a member of ESA's SAR Quality Working Group. Together with Erich Meier, he leads the SAR Group, Remote Sensing Laboratories. His research is in the fields of SAR polarimetry and interferometry, as well as geometric and radiometric calibration of SAR imagery.

Erich Meier (M'09) received the M.Sc. degree in geography and the Ph.D. (Hons.) degree in remote sensing from the University of Zurich, Zurich, Switzerland, in 1982 and 1989, respectively.

From 1979 to 1982, he was a Research Assistant with the Remote Sensing Section and, from 1982 to 1983, with the GIS Laboratory, Department of Geography. From 1983 to 2006, he was a Research Scientist with the Remote Sensing Laboratories (RSL), University of Zurich, where he is currently involved in teaching, as well as digital image processing, software development for computer graphics, and radiometric and geometric calibration of SAR and optical imagery. Since 2000, he has been the Head of SARLab, a research group within RSL. The main research interests of this group are the development of new focusing algorithms for SAR data from UHF to millimeter wave, interferometry, polarimetry, and MTI algorithms, as well as calibration/validation activities for spaceborne and airborne systems. He is responsible for the research strategies as well as the team organization.